

Trapping Conformational Intermediate States in the Reaction Center Protein from Photosynthetic Bacteria[†]

Qiang Xu and M. R. Gunner*

Department of Physics, Room J419, City College of New York, 138th Street and Convent Avenue, New York, New York 10031

Received October 4, 2000; Revised Manuscript Received January 8, 2001

ABSTRACT: In protein, conformational changes are often crucial for function but not easy to observe. Two functionally relevant conformational intermediate states of photosynthetic reaction center protein (RCs) are trapped and characterized at low temperature. RCs frozen in the dark do not allow electron transfer from the reduced primary quinone, Q_A^- , to the secondary quinone, Q_B . In contrast, RCs frozen under illumination in the product ($P^+Q_AQ_B^-$) state, with the oxidized electron donor, P^+ , and reduced Q_B^- , return to the ground state at cryogenic temperature in a conformation that allows a high yield of Q_B reduction. Thus, RCs frozen under illumination are found to be trapped above the ground state in a conformation that allows product formation. When the temperature is raised above 120 K, the protein relaxes to an inactive conformation which is different from the RCs frozen in the dark. The activation energy for this change is 87 ± 8 meV, and the active and inactive states differ in energy by only 16 ± 3 meV. Thus, there are several conformational substates along the reaction coordinate with different transition temperatures. The ground state spectra of the RCs in active and inactive conformations report differences in the intraprotein electrostatic field, demonstrating that the dipole or charge distribution has changed. In addition, the electrochromic shift associated with the Q_A^- to Q_B electron transfer at low temperature was characterized. The electron-transfer rate from Q_B^- to P^+ was measured at cryogenic temperature and is similar to the rate at room temperature, as expected for an exothermic, electron tunneling reaction in RCs.

Conformational flexibility is important for the function of proteins (1, 2). At room temperature, proteins fluctuate among many conformational states. At low temperature, proteins will become trapped in harmonic motions near the conformation it was frozen into (3–9). Intraprotein reactions are inhibited if this conformation cannot access the transition state. When the temperature is raised, relaxation between conformational substates becomes possible. Elastic incoherent neutron scattering and X-ray crystallography measurements of bacteriorhodopsin (10) and myoglobin (4) show that different parts of the protein relax at different temperatures (11).

Bacterial photosynthetic reaction center protein (RCs)¹ has a number of physiological electron tunneling reactions that occur even at cryogenic temperatures. This system can therefore be used to characterize conformational substates of physiologically important reactions. Previous studies of

RCs have characterized the protein at cryogenic temperatures. RCs can be trapped in a distribution of substates which exhibit a wider distribution of reaction rates (12, 13). Other studies have characterized unrelaxed product states (14). In addition, reactions that normally do not occur at low temperatures have been observed when the protein is frozen into appropriate conformational states (12).

The bacterial photosynthetic reaction center is the membrane protein that facilitates the conversion of light energy to chemical energy. Upon absorption of a photon, a separation of charge is achieved by a series of electron transfers between the cofactors bound to the protein. (For reviews, see refs 15–17.) Charge separation starts with a very fast picosecond electron transfer from the primary electron donor P, a dimer of bacteriochlorophyll, to the bacteriopheophytin on the L branch of the protein, BPh_L , followed by a slower reduction (~ 200 ps) of the primary quinone, Q_A . The electron is then transferred to the secondary quinone, Q_B . When no external electron donor is present, the electron returns to P^+ , and the system is restored to the ground state (Figure 1).

At cryogenic temperatures charge separation to form $P^+Q_A^-$ and charge recombination to regenerate the ground state occurs with rates and yields little different than found at room temperature. However, at low temperatures, the electron transfer from Q_A^- to Q_B stops, demonstrating that some activated step limits this electron transfer. Kleinfeld et al. (12) observed previously that RCs frozen under illumination in the $P^+Q_B^-$ state and then allowed to return

[†] We are grateful for the financial support of the Department of Agriculture (CREES 1999-01256) and for NIH RCMI Grant RR03060 for maintenance of central facilities.

* To whom correspondence should be addressed. Telephone: 212-650-5557. Fax: 212-650-6940. E-mail: gunner@sci.cuny.cuny.edu.

¹ Abbreviations: RC, reaction center; Q_A and Q_B , primary and secondary quinone electron acceptors; P, bacteriochlorophyll dimer which is the primary electron donor; BPh_L and BPh_M , bacteriopheophytin associated with the L and M subunits, respectively, BCh_L and BCh_M , bacteriochlorophyll monomer in the L and M subunits; LDAO, lauryldimethylamine *N*-oxide; UQ10, ubiquinone-10 (2,3-dimethoxy-5-methyl-6-decylpropyl-1,4-benzoquinone); UQ1, ubiquinone-1; MQ4, 2-methyl-3-phytyl-1,4-naphthoquinone. CCD, charge-coupled device.

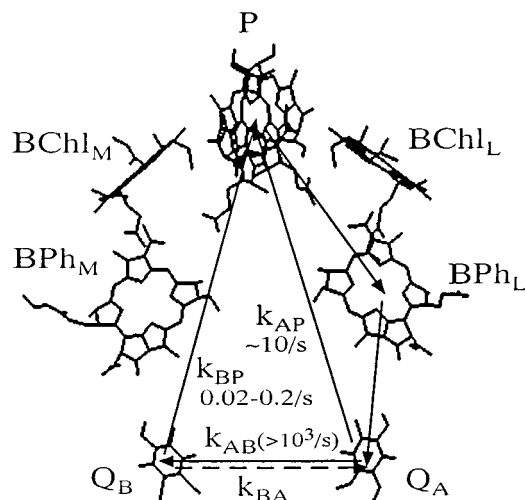


FIGURE 1: Cofactor arrangement and electron-transfer pathway in *Rb. sphaeroides* RCs. At room temperature, the electron on Q_B^- returns to P^+ by thermal repopulation of the $P^+Q_A^-$ state. At cryogenic temperature, the direct tunneling at k_{BP} is seen. Approximate rate constants at cryogenic temperatures in the light-adapted protein are given. The values for k_{BP} and k_{AP} (12, 13) were determined directly. The value for k_{AB} is estimated from the high quantum yield of $P^+Q_B^-$ formation.

to the ground state can support electron transfer from Q_A^- to Q_B . Thus, RCs can be trapped in an activated conformation. It is this observation that will be explored here.

The importance of conformational change in the Q_A^- to Q_B electron transfer has also been seen in kinetic studies at room temperature. Two kinetic phases can be found (18, 19). The slower ($\tau \approx 100 \mu\text{s}$) is independent of the driving force, indicating that the electron transfer itself is not rate limiting and that the reaction is gated by some other process (20). This is the predominant process in isolated, native RCs. The faster rate ($\tau < 10 \mu\text{s}$) depends on the driving force as predicted by Marcus electron-transfer theory (21), indicating that RCs can be prepared where the gate is open and that the electron transfer itself determines the rate. Binding a Zn^{2+} or Cd^{2+} ion to a surface site on the RCs slows the $100 \mu\text{s}$ phase of the Q_A^- to Q_B electron transfer. Thus ion binding impedes the rate-limiting conformational change (22, 23).

High-resolution X-ray crystal structures can follow significant, heavy atom conformational changes along a reaction coordinate if an intermediate state can be trapped (24–27). RC structures have been obtained at 2.2 and 2.6 Å resolution of the protein frozen in the dark in the ground state and under illumination in the $P^+Q_B^-$ state. Comparison reveals some structural differences even at this resolution, the most significant being that Q_B occupies a site 3.5 Å closer to Q_A in crystals frozen in the light rather than in the dark (28). However, other processes may also contribute to the temperature dependence of Q_B reduction which could not be seen at the resolution of these structures. Experimental and computational studies suggest that proton transfer, changes in hydrogen bond patterns, and side chain reorientation need to occur for the electron transfer from Q_A^- to Q_B to be energetically favorable (29–34).

To further characterize the conformational gating that controls electron transfer from Q_A^- to Q_B , RCs were trapped in an active state by freezing under illumination using methods developed by Kleinfeld et al. (12). The loss of

activity in the dark-adapted protein follows the temperature dependence of the rate of reduction of Q_B . The stability of the active conformation at different temperatures probes the shape of the energy landscape near the active conformation. Electrochromic shifts that monitor changes in the electrostatic fields in the protein are compared in the ground states of light- and dark-adapted protein as well as in the $P^+Q_A^-$ and $P^+Q_B^-$ states at low temperature. In addition, the temperature dependence of the charge recombination reaction from $P^+Q_B^-$ to the ground state is characterized.

MATERIALS AND METHODS

Engineered polyhistidine-tagged, carotenoid-containing, *Rhodospirillum rubrum* reaction centers were purified utilizing the high-affinity interaction between the polyhistidine tag and Ni-NTA (nitrilotriacetic acid) resin (35). Non-His-tagged carotenoid-less strain R-26 RC was also used for comparison with previous measurements. No significant difference between the two strains was observed in the measurements reported here. The non-His-tagged protein was isolated following established procedures using lauryldimethylamine *N*-oxide (LDAO) extraction and purified using ammonium sulfate and DEAE (diethylaminoethyl) chromatography (36). The Q_B site is less than 5% occupied after either purification. Protein for Q_A reconstitution has the native ubiquinone-10, Q_A , extracted with 4% LDAO and 10 mM *o*-phenanthroline using the method of Okamura (37) with minor modification (38). After this treatment, the quinone content is $Q_B = 0\%$ and $Q_A \leq 5\%$. The residual LDAO concentration from the RC stock solution is 0.025%.

Quinones added to the RCs, ubiquinone-10 (UQ10), ubiquinone-1 (UQ1), and menaquinone-4 (MQ4), were dissolved in 2% Triton X-100. The relatively insoluble UQ10 stock solution was heated for 5 s in a microwave oven before being added to the RCs. To reconstitute Q_A activity with MQ4, about 1.5 MQ4 per RC was added. Q_B was reconstituted with 15–20 UQ10 or UQ1 per RC (39). RCs with MQ4 at Q_A and UQ10 at Q_B were prepared as described previously (21).

Flash-induced absorbance transients were measured with a flash spectrophotometer of local design. The sample was excited by a 2.2 J, 10 μs flash from a xenon flash lamp. A low-pass filter with cutoff of 750 nm (Oriel) filtered out the shorter wavelengths. The transmitted light was detected by a Thorn EMI 9798QB photomultiplier. The electron-transfer kinetics were monitored by following the difference in P and P^+ absorbance at 430 nm.

Absorbance changes from 700 to 950 nm were measured with a liquid nitrogen cooled CCD detector (Princeton Instrument, LN/CCD-1024-EHRB/1). A weak, nonactinic xenon flash lamp ($\sim 0.4 \mu\text{s}$ fwhm) (IBH Consultants, 5000XeF) provided the measuring light. The transmitted light was focused onto an optical fiber and into the spectrometer (Jobin-Yvon, HR460) with the CCD detector at the image plane. The absorbance was calculated by comparing the light transmitted through a buffer solution (I_0) and through the RCs after excitation $I(t)$ at the same temperature. $A(t) = \log(I_0/I(t))$. The delay between the pump and probe flash was varied with a delay generator (Stanford Research DG535) to follow the time dependence of the reaction. As the absorbance changes are collected in the same spectral region

as the exciting flash, a minimum delay of 20 ms was needed to give the CCD time to remove the charges induced by the actinic flash.

The low-temperature measurements were carried out in a closed cycle helium cryostat system (APD cryogenics, CSW202A) with a programmable temperature controller. The temperature resolution is 0.1 K and controllability is ± 0.4 K.

For low-temperature experiments, RCs in Tris buffer were mixed with 2 volumes of glycerol. The final RC concentration was 3–4 μM for single-wavelength kinetics measurements and 30 μM for time-resolved spectral measurements. The optical cell has a light path of 1 mm. The actinic light and measuring light were perpendicular to each other with an incident angle of 45° at the sample.

Two different methods were used to trap the protein in the light-induced $\text{P}^+\text{Q}_\text{B}^-$ conformation. Following the method used by Kleinfeld et al. (12), the sample was plunged into liquid nitrogen for about 3 s while under illumination and then transferred to the cryostat at 40 K. The sample was dark adapted for 30 min at 40 K to let the RCs re-form the ground state and then brought to the measurement temperature. Helium gas was blown through the chamber when frozen samples were placed in the precooled system. The cryostat temperature was found to increase by 40 K or less and then return to the set temperature in about 3 min. The protein was also trapped by cooling the sample slowly (at ≈ 5 K/min) under a 75 W continuous xenon light or with actinic flashes repeated at 1 Hz. A 675 nm low-pass filter (Corion) was used in either case.

When RCs are activated at any temperature with an actinic flash, $\text{P}^+\text{Q}_\text{A}^-$ is formed. This can either yield $\text{P}^+\text{Q}_\text{B}^-$ by electron transfer from Q_A^- to Q_B (k_{AB}) or return to the ground state at k_{AP} (Figure 1). The quantum efficiency of $\text{P}^+\text{Q}_\text{B}^-$ formation reflects the competition between these two steps. In dark-adapted samples k_{AB} slows with temperature so that the rate can be estimated from the quantum efficiency, ϕ , of $\text{P}^+\text{Q}_\text{B}^-$ formed from $\text{P}^+\text{Q}_\text{A}^-$, where ϕ is

$$\phi = \frac{k_{\text{AB}}}{k_{\text{AB}} + k_{\text{AP}}} = \frac{[\text{P}^+\text{Q}_\text{B}^-]_{t=0}}{[\text{P}^+\text{Q}_\text{A}^-]_{t=0} + [\text{P}^+\text{Q}_\text{B}^-]_{t=0}} \quad (1)$$

Over the temperature range when k_{AB} and k_{AP} are comparable, ϕ differs from 0 and 1.0, and eq 1 can be used to derive k_{AB} . ϕ for $\text{P}^+\text{Q}_\text{B}^-$ formation is the fraction of excited RCs that form $\text{P}^+\text{Q}_\text{B}^-$. This can be readily determined from the kinetics of reduction of P^+ which occurs at very different rates from the $\text{P}^+\text{Q}_\text{A}^-$ and $\text{P}^+\text{Q}_\text{B}^-$ states. The rate k_{AP} has been well characterized, increasing from 9 to 37 s^{-1} as the temperature is lowered from room temperature to 5 K (12, 13, 40). In contrast, once formed, $\text{P}^+\text{Q}_\text{B}^-$ returns to the ground state at rates between 1 and 0.02 s^{-1} .

The use of ϕ to determine k_{AB} can be tested by exciting a sample when most of the $\text{P}^+\text{Q}_\text{A}^-$ RCs have returned to the ground state but the $\text{P}^+\text{Q}_\text{B}^-$ RCs have not. The second flash re-forms $\text{P}^+\text{Q}_\text{A}^-$, of which a fraction ϕ should generate additional $\text{P}^+\text{Q}_\text{B}^-$. The yield of $\text{P}^+\text{Q}_\text{B}^-$ should be the same on each flash if the competition between k_{AB} and k_{AP} is the sole cause of the low $\text{P}^+\text{Q}_\text{B}^-$ yield. Here caution must be taken to correct for the incomplete saturation of the actinic

light so that not all RCs form $\text{P}^+\text{Q}_\text{A}^-$ in a single flash and also for the portion of the RCs without bound Q_B .

When the temperature of light-adapted RCs is raised above 120 K, the trapped conformation which can form $\text{P}^+\text{Q}_\text{B}^-$ relaxes so that only the faster decaying $\text{P}^+\text{Q}_\text{A}^-$ RCs are seen after a flash. The relaxation rate was measured at different temperatures. Starting at 40 K it takes ≈ 15 min to reach 200 K. The time at which the temperature reading reaches the set value is used as time zero. The position of the temperature and optical measurements are separated by about 0.5 cm.

For measurements at constant temperature, 5–10 flashes approximately 20 min apart were averaged. No averaging was carried out for the measurement of the relaxation processes in the 120–200 K temperature region.

The $\text{P}^+\text{Q}_\text{B}^-$ charge recombination kinetics were analyzed by two exponential decays plus a constant using a nonlinear least-squares fitting program of the Levenberg–Marquardt algorithm (Igor Pro from WaveMetrics). The constant is 10% or less of the total amplitude. A more general distributed rate model can also be used to analyze this type of kinetics (41) where

$$\Delta A(t) = \Delta A(0) \int_0^\infty D(k) e^{-kt} d \log k \quad (2)$$

$D(k)$ is the distribution of rates on the log k scale. This Laplace transformation can be inverted numerically using the Tikhonov–Miller regularization method (42).

RESULTS

RCs Trapped in the Dark-Adapted Conformation. At low temperature, flash excitation yields $\text{P}^+\text{Q}_\text{A}^-$ in essentially 100% of the RCs (43). $\text{P}^+\text{Q}_\text{A}^-$ returns to the ground state at ~ 9 s^{-1} (k_{AP}). When the electron is transferred to Q_B , charge recombination slows to < 1 s^{-1} at room temperature and becomes even slower at lower temperature (see below). Thus, it is possible to differentiate between RCs in $\text{P}^+\text{Q}_\text{A}^-$ and $\text{P}^+\text{Q}_\text{B}^-$ states by monitoring the rate at which the P^+ formed on a flash is rereduced to P at 430 or 890 nm. As the temperature is lowered, the slow component of charge recombination is lost (Figure 2) (44). In native RCs at pH 8.0 (67% glycerol), the quantum yield of $\text{P}^+\text{Q}_\text{B}^-$ (ϕ) is 50% at ~ 225 K. At this temperature $k_{\text{AB}} = k_{\text{AP}} \approx 10$ s^{-1} .

An estimate of the activation energy of 8 ± 1 kcal/mol for k_{AB} can be derived from the temperature dependence of quantum efficiency (Figure 2). Equation 1 is used to estimate k_{AB} from ϕ for $\text{P}^+\text{Q}_\text{B}^-$ formation. Between 250 and 180 K electron transfer from Q_A^- to Q_B (k_{AB}) slows to where it can no longer compete with k_{AP} [$k_{\text{AB}} \gg k_{\text{AP}}$ ($\phi \approx 1$) to $k_{\text{AB}} \ll k_{\text{AP}}$ ($\phi \approx 0$)] (Figure 2) (12, 45). Equation 1 makes the simplification that the electron transfer from Q_A^- to Q_B happens at a single exponential rate. Direct measurement indicates that the Q_A^- to Q_B kinetics become more inhomogeneous when temperature is lowered (18). Therefore, the rate obtained from eq 1 represents a weighed average, and the derived activation energy is a rough estimate of the true value. Given a single enthalpy barrier, the error will be small if the energy distribution of RCs is much smaller than the activation energy itself.

RCs Trapped in Light-Adapted Conformations. When RCs are frozen under illumination, three populations are seen after

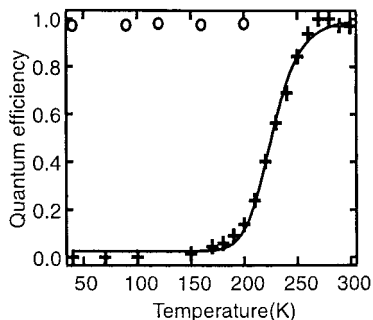


FIGURE 2: Fraction of RCs that show the slow, $P^+Q_B^-$ component of P^+ decay after an actinic flash. $[RC] = 4 \mu M$ and $pH = 8.0$. For RCs frozen in dark, the amplitude was normalized against the value at 300 K. For RCs frozen under illumination, the maximum amplitude after 10 flashes (0.1 s interval) is taken as 1. Such normalization corrects for the portion of RCs without bound Q_B or RCs trapped in an inactive state. The falloff in Q_B reduction in the dark-adapted RCs is fit using eq 1, assuming that k_{AP} is temperature independent and k_{AB} is an activated process, $k_{AB} = k_0 \exp(-E_a/kT)$. k_{AP} is $9 s^{-1}$ and k_{AB} is $10^4 s^{-1}$ at 300 K (19). If the process has a single activation energy of 8 kcal/mol (340 meV), k_{AP} will equal k_{AB} and the quantum efficiency will be 50% at ~ 225 K.

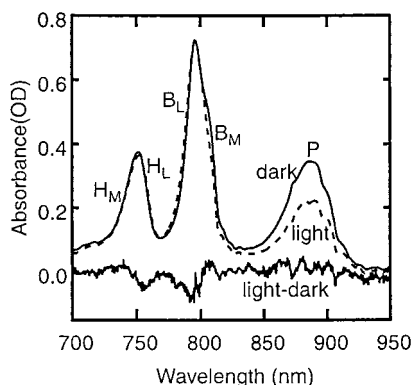


FIGURE 3: Spectrum of the RC ground state for protein frozen in the dark (solid line) and under illumination (dashed line). The peak assignments are from ref 46. The difference between the two spectra is also shown. The difference spectrum is corrected for a trapped population of P^+ as described in the text. $[RC] = 31 \mu M$ and $T = 40$ K.

dark adaption. The near-IR spectrum shows a loss of the 890 nm P absorbance, indicating that some RCs are trapped in an inactive state where P^+ remains oxidized (Figure 3). At 110 K, no change in this spectrum is observed in 24 h. This inactive fraction has been seen previously (45) and may represent RCs frozen in a $P^+Q_A^-Q_B$ state where the quinone has been oxidized by adventitious mediators (12). Generally, the stronger the illumination during freezing, the more RCs trapped. The protein is not permanently damaged as it regains activity when thawed. This population will not be discussed further.

Under conditions used here more than 80% of the protein which is frozen in a charge-separated state returns to the ground state after 30 min at low temperature. After an actinic flash two kinetic components are now seen for P^+ rereduction. Approximately, 10% of the RCs lack Q_B . These form only the $P^+Q_A^-$ state, which decays back to the ground state at the characteristic 10 s (40 K) after a flash. In a given sample, the fraction of RCs without Q_B at low temperature is unchanged, within 10% of that found at room temperature.

As has been seen previously (12), RCs with bound Q_B frozen under illumination adopt a ground state conformation

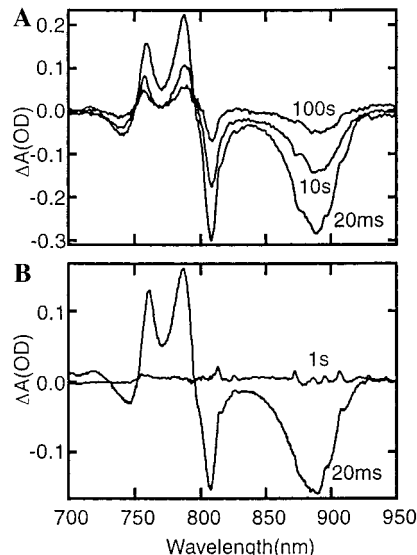


FIGURE 4: Time dependence of the absorption change at 40 K after an actinic flash in RCs frozen under illumination (A) and in the dark (B) at 40 K. The narrow peaks, most prominent in the 1 s trace (panel B), are lines in the weak xenon measuring flash. Five transients were averaged at each time.

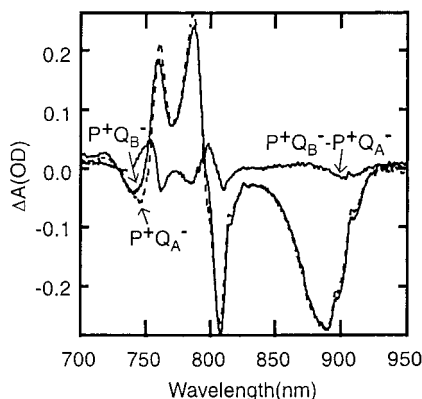


FIGURE 5: Comparison between the light-induced absorption change in RCs frozen under illumination ($P^+Q_B^-$) and in the dark ($P^+Q_A^-$) at 40 K. The spectra are normalized to match the P^+ signal at 890 nm. The difference shows the shifts in the cofactor spectra in the presence of Q_B^- instead of Q_A^- .

that supports electron transfer from Q_A^- to Q_B . In these RCs the P^+ formed by an actinic flash decays back to the ground state in tens of seconds (Figure 4A). In contrast, the absorbance change decays to 0 in less than 1 s in RCs frozen in the dark (Figure 4B). The quantum efficiency, ϕ , of the electron transfer, determined with the multiple flash method, is greater than 98% in the light-adapted RCs at 40 K. Given the known k_{AP} value of about $10 s^{-1}$ in the light-adapted RCs at 40 K (12), k_{AB} in the active conformation must be faster than $\sim 10^3 s^{-1}$ (eq 1). The spectral changes associated with the slow phase are consistent with those expected for $P^+Q_B^-$ returning to the ground state.

The double difference spectrum ($\Delta\Delta A$) of the flash absorption change in RCs frozen under illumination (ΔA_L) and in the dark (ΔA_D) is $\Delta\Delta A = \Delta A_L - n\Delta A_D$ (Figure 5). This difference between the $P^+Q_B^-$ minus ground state spectrum (ΔA_L) and the $P^+Q_A^-$ minus ground state spectrum (ΔA_D) provides the spectral difference between RCs with Q_B^- and Q_A^- . The normalization factor, n , matches the absorbance change in the two samples at 890 nm. This

corrects for the activity lost in the light-adapted samples as well as for the decay of the P^+ signal during the 20 ms between the actinic and measuring flashes. The latter is a small factor in the $P^+Q_B^-$ RCs but is more significant in the $P^+Q_A^-$ RCs.

The near-IR spectra of RCs are dominated by the absorbance bands of the bacteriochlorophyll dimer (P), monomers (B_L and B_M), and bacteriopheophytins (H_L and H_M) (see Figure 3). The features of the double difference spectrum, where the changes at P are subtracted out, show band shifts that result from changes in the electric field at each chromophore. The spectrum qualitatively agrees with the Q_B^- minus Q_A^- spectrum at room temperature (18). However, because the absorption bands are much narrower at 40 K, more features are seen. From previous assignments of the absorption peaks for each species (46, 47), the major features in the spectrum can be tentatively assigned (Figures 3 and 5). The difference spectrum shows an ≈ 15 cm^{-1} blue shift of $BChl_M$ and BPh_L and a comparable red shift for $BChl_L$ and BPh_M . From the orientation of the four chromophores, this indicates an increase of the field intensity at $BChl_M$ and BPh_M and a decrease at $BChl_L$ and BPh_L . These shifts are consistent with the negative charge moving from Q_A to Q_B , reducing the distance to the M-side cofactors and increasing it to the L-side cofactors. The broad feature near 900 nm indicates some absorption change on the red side of P^+ . This could represent either some relaxation process near P or a difference between its long-range electrostatic interaction with Q_A^- and Q_B^- .

Some changes must be trapped in the RCs frozen in the light to allow electron transfer from Q_A^- to Q_B . The difference between the ground state spectrum of RCs frozen in the light and the dark was measured to see if the electrostatic fields throughout the protein are different (Figure 3). One complication here is that the population of RCs trapped in the inactive P^+ state also contributes to this difference spectrum. But as mentioned previously, the percentage of the RCs trapped in the inactive P^+ state can be varied by changing the illumination conditions. When spectra with different percentages of the two species are compared, the spectrum of the trapped RCs and the difference of the ground states for the light- and dark-adapted ground state spectra (Figure 3) can be separated.

Although the signal-to-noise ratio is not ideal, there appears to be an electrochromic shift of the bacteriopheophytin (BPh) and monomer bacteriochlorophyll (BChl) bands when RCs are frozen in the light. The electrochromic shift of the bacteriopheophytin (BPh) and monomer bacteriochlorophyll (BChl) bands is caused by a change in the electrical field at the chromophores, i.e., a Stark shift. These shifts have been analyzed in detail for the $P^+Q_A^-$ charge separation (47). The shift caused by freezing RCs in the light is in the opposite direction from that induced by the $P^+Q_A^-$ or $P^+Q_B^-$ charge separation, indicating a difference in the electric field at the chromophores which is opposite to that induced by $P^+Q_A^-$ or $P^+Q_B^-$. The extra field's projection on the transition dipole of BPh or BChl can be estimated from the magnitude of the shift, which is proportional to the height of the difference signal when the shift is small compared to the width of the peak. The change in the field projection is about 20% of that found for the $P^+Q_A^-$ or $P^+Q_B^-$ charge-separated states.

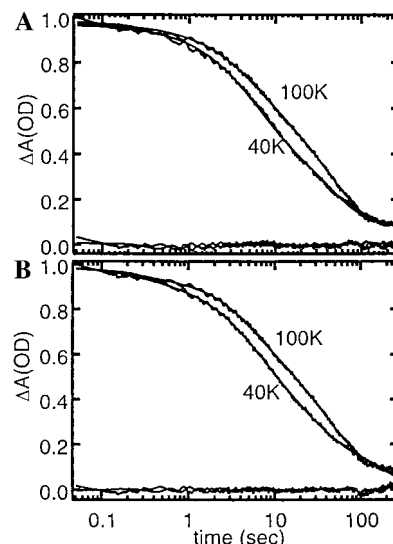


FIGURE 6: Kinetics of the $P^+Q_B^-$ charge recombination fitted by (A) double exponential fit and by (B) distributed rate model (eq 2). The lines at the bottom are the residuals from each fit. The fitting parameters for (A) are given in Figure 7.

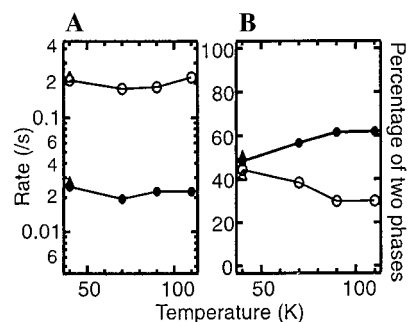


FIGURE 7: Temperature dependence of the two components for the $P^+Q_B^-$ charge recombination from the double exponential fit: (A) rates; (B) amplitude. Filled symbols indicate the slower component and open symbols the faster rate: circle, $UQA-UQB$; triangle, $MQA-UQB$ (40 K only).

$P^+Q_B^-$ Charge Recombination Kinetics. In light-adapted RCs, the $P^+Q_B^-$ charge recombination kinetics can be examined in detail at low temperature for the first time. The rate of this reaction was measured at 430 nm, monitoring the change of the P absorbance (Figure 6). At 40 K the kinetics can be fit with two exponentials at 0.21 and 0.025 s^{-1} and a constant which is less than 10% of the total amplitude. Since the two rates differ by more than 10-fold, they can be easily separated in the kinetic analysis (Figure 6A).

The kinetics were also analyzed with a distributed rate model as eq 2 (Figure 6B). The distribution has rates centered around the same two values obtained in the two exponential fit. There may be a slightly broader distribution of the faster rate (data not shown). However, Figure 6 shows that the residual with the simpler, two exponential fit is comparable to that found with a distribution of exponential decays. Both charge recombination rates show little temperature dependence from 40 to 110 K (Figure 7A). However, the fraction of the reaction at the faster rate decreases from 44% to 30% as the temperature is raised (Figure 7B).

Since the light-induced product state has a long lifetime, one practical concern is whether the weak measuring light will cause some RCs to be trapped in the product state,

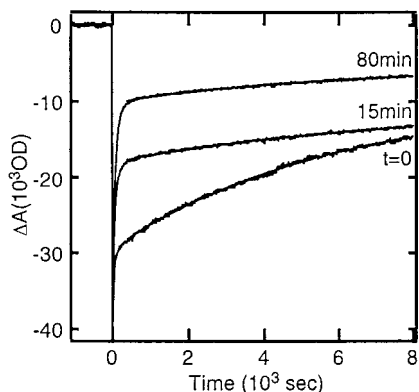


FIGURE 8: Charge recombination kinetics after the RCs trapped in the active state are warmed to 160 K from 40 K. $t = 0$ is the time when the thermometer reading reaches 160 K. The RCs return quickly to the ground state from $P^+Q_A^-$, while those that form $P^+Q_B^-$ show much slower charge recombination. The difference in the $P^+Q_B^-$ charge recombination kinetics at early time might be due to a difference in the relaxation rates of the two substates of the active conformation. The traces were fitted with two exponentials plus a constant fixed at 10% of the total amplitude. The fractional constant is estimated from measurements on a longer time scale. The fitting parameters are as follows: $t = 0$, $k_1 = 0.20 \text{ s}^{-1}$ (55%), $k_2 = 0.02 \text{ s}^{-1}$ (35%); $t = 15 \text{ min}$, $k_1 = 0.27 \text{ s}^{-1}$ (22%), $k_2 = 0.02 \text{ s}^{-1}$ (68%); $t = 80 \text{ min}$, $k_1 = 0.28 \text{ s}^{-1}$ (28%), $k_2 = 0.02 \text{ s}^{-1}$ (62%).

distorting the measured kinetics. To assess the contribution of the measuring light, its intensity was varied by 10-fold around the value normally used, from approximately 10^{11} to 10^{12} quanta/s. The charge recombination kinetics were independent of the measuring light intensity (data not shown).

There are two pathways for charge recombination in $P^+Q_B^-$ RCs. One is by electron tunneling from Q_B^- to P^+ . However, at room temperature, $P^+Q_B^-$ charge recombination proceeds predominantly via $P^+Q_A^-$ as an intermediate (44, 48). The rate is therefore dependent on a preequilibrium between the $P^+Q_A^-$ and $P^+Q_B^-$ and so is sensitive to the energy level of Q_A^- (21, 49). The $P^+Q_B^-$ charge recombination rate was measured at 40 K in RCs with MQ4 rather than UQ10 as Q_A . Q_B is still UQ10. The free energy of the $P^+Q_A^-$ state with MQ4 is 30 meV higher than with UQ10. If charge recombination depends on the thermal equilibration of $P^+Q_A^-$ and $P^+Q_B^-$ as it does at room temperature, the rate would be expected to slow by more than 1000-fold at 40 K. However, the measured rate is independent of the energy of the $P^+Q_A^-$ state (Figure 7). Thus, the contribution of this indirect route to the $P^+Q_B^-$ charge recombination is negligible, and the reaction proceeds at a Q_A -independent process via direct tunneling from Q_B^- to P^+ .

Relaxation of the Active, Light-Adapted Conformation. Light-adapted RCs remain capable of forming $P^+Q_B^-$ on a flash for at least 24 h at temperatures below 70 K. However, when the temperature is then raised, the protein begins to relax to an inactive conformation. There is no loss in the initial charge separation reaction since the amount of P^+ formed remains almost unchanged (Figure 8). However, with time the amplitude of the slow, $P^+Q_B^-$, charge recombination decreases and that of the fast, $P^+Q_A^-$, component increases. The kinetics of $P^+Q_B^-$ charge recombination can be fitted with a two exponential decay with similar rates as at lower temperature. Figure 8 shows that the percentage of the slower kinetic phase seems smaller than expected at early times.

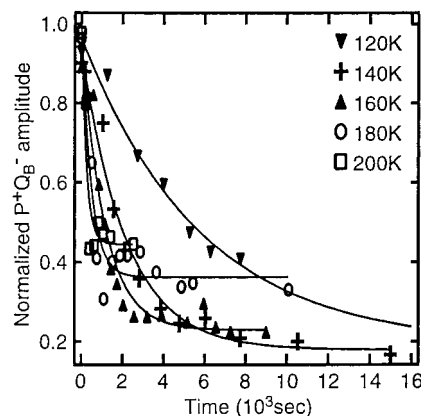


FIGURE 9: Percentage of the $P^+Q_B^-$ component in the charge recombination kinetics as a function of time. The RCs were frozen under illumination to 40 K, equilibrated for 30 min, and brought up to the measuring temperature in 10–15 min. The relaxation of the active, light-adapted RCs into a conformation where $P^+Q_B^-$ is not formed is fitted to an exponential decay at each temperature.

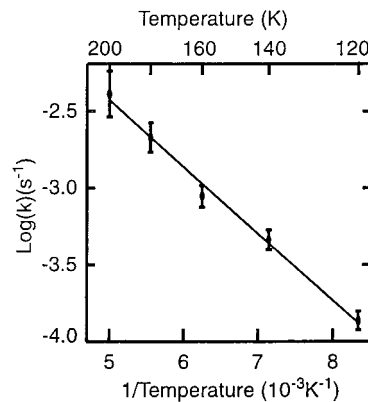


FIGURE 10: Temperature dependence of the relaxation of light-adapted RCs into an inactive conformation (Figure 9). The activation energy is $87 \pm 8 \text{ meV}$, and the extrapolated rate at infinite temperature is 2 s^{-1} .

This might be caused by difference in the relaxation rate of the two substates of the active conformation. The relaxation rate becomes faster as the temperature is raised (Figure 9). The van't Hoff plot of $\log k$ versus $1/\text{temperature}$ indicates the activation energy for inactivation is $87 \pm 8 \text{ meV}$ (Figures 10 and 11).

As the RCs frozen in the light are allowed to come to equilibrium at temperatures between 120 and 200 K, some $P^+Q_B^-$ activity remains even after 24 h. Thus, at these temperatures an equilibrium is set up between active and inactive conformations. As the temperature is raised, the active fraction is larger. The multiflash method shows that the fractional activity does not represent a homogeneous population of RCs with a quantum yield less than 1, since a second actinic flash 1 s after the first yields no additional $P^+Q_B^-$. Rather, the system relaxes into a slowly equilibrating mixture of active and inactive ground state conformations.

The equilibrium constants derived from the ratio of the active and inactive conformations between 160 and 200 K yield a free energy difference of $16 \pm 3 \text{ meV}$. At 120 and 140 K the free energy difference is smaller (4 and 8 meV, respectively). This may be caused by an overestimate of the active conformation because the very slow reaction does not reach equilibrium at these temperatures. The RCs frozen in

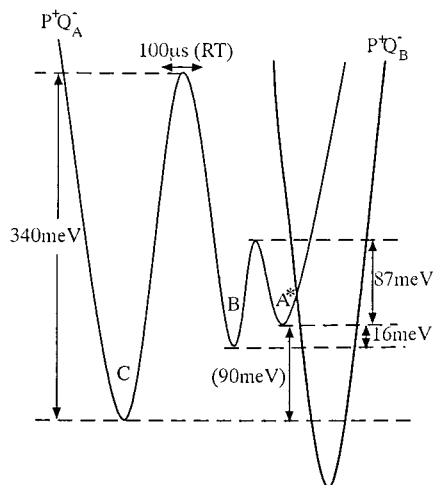


FIGURE 11: Model of the three conformational states characterized here. In dark-adapted RCs, the protein is trapped in the inactive C conformation. In light-adapted RCs, the protein is trapped in the active A* conformation. When RCs trapped in the active conformation are warmed above 120 K, the protein relaxes into another inactive state, B, which remains in equilibrium with A*. The free energy difference between A* and C is derived from the model of Li et al. (21). The activation energy between C and A* is estimated from the data in Figure 2.

the dark show no Q_B activity in this temperature range. Thus this relaxed conformation represents a previously unobserved intermediate state different from both the dark-adapted and active light-adapted conformations.

The most obvious conformational change between the RCs frozen in the dark and light in the crystallographic study is the position of the quinone (28). Therefore, the quinone movement was suggested to be the rate-limiting conformational change. To check whether quinone movement is involved in the relaxation of the active conformation between 120 and 200 K, UQ1, which has a much shorter isoprene tail, was also used as Q_B . A much faster relaxation rate might be expected if rotation of the bulky tail limits the movement of the native quinone. Instead, similar relaxation rates were observed with UQ1 or UQ10 as Q_B .

DISCUSSION

When reaction centers (RCs) are frozen in dark, the yield of electron transfer from Q_A^- to Q_B diminishes with temperature so that almost no reaction is seen below 200 K. In contrast, in RCs frozen under illumination the reaction proceeds with high yield even at 50 K (12). Thus, RCs frozen in the $P^+Q_B^-$ state must retain some conformational changes at low temperature so they return to the ground state in an altered conformation that now supports rereduction of Q_B . Below 70 K the dark- and light-adapted structures remain trapped for days. Between 120 and 200 K the active conformation relaxes into a nearby inactive state. There is an 87 meV activation energy for this relaxation. Active and inactive RCs remain in equilibrium in this temperature range. In contrast, in protein frozen in the dark there is no activity at these temperatures. The relationship between the active and two inactive conformations is summarized in Figure 11.

The Charge Recombination Rate in the Light Conformation Is Consistent with Direct Electron Transfer from Q_B^- to P^+ . The earliest observation that RCs could be frozen into an active conformation was made by Kleinfeld et al. (12).

The general results reported here are in good agreement with that earlier study. The one significant difference in the observations is that $P^+Q_B^-$ returns to the ground state here much faster than previously reported and at a rate that is temperature independent. The reason for the discrepancy is not clear, but the result presented here seems to be more consistent with that found for other electron tunneling processes in RCs at low temperature.

At room temperature, charge recombination in $P^+Q_B^-$ RCs proceeds at $\sim 1 \text{ s}^{-1}$ predominantly via the intermediate state of $P^+Q_A^-$. The direct electron transfer from Q_B^- to P^+ is much slower. The latter mechanism only becomes important when the free energy of either Q_A or Q_B is altered by quinone replacement (50–52) or by mutation (49, 50, 53) to make electron transfer via the indirect route slower than the direct route. The direct electron transfer from Q_B^- to P^+ occurs at $0.12\text{--}0.19 \text{ s}^{-1}$ at room temperature (50–53). Charge recombination in $P^+Q_B^-$ RCs in the light-adapted conformation at cryogenic temperature shows two phases at 0.2 and 0.02 s^{-1} with comparable amplitudes. The faster rate is similar to that seen at room temperature. At low temperature the conversion between the two states producing the two rates is much slower than charge recombination. If the equilibration becomes faster at room temperature, the observed rate would be close to that of the faster component. Therefore, the rate of electron tunneling from Q_B^- to P^+ appears to be essentially temperature independent.

This measurement of the direct tunneling along the M branch of the RCs from Q_B^- to P^+ at cryogenic temperature can be compared with the well-characterized charge recombination along the L branch of the protein from Q_A^- to P^+ . Both processes are somewhat biphasic, although the difference in rates is larger for the electron transfer from Q_B^- to P^+ than from Q_A^- (14, 54–56). In RCs frozen in the light in the absence of Q_B , Q_A^- to P^+ electron transfer is better analyzed by a distribution of exponentials than by one or two exponentials (12, 13). In contrast, in light-adapted RCs the Q_B^- to P^+ reaction remains well characterized by two exponentials (Figure 6A).

The Q_B^- to P^+ reaction is independent of temperature below 110 K, and the low-temperature rate is comparable to that found at room temperature. This is again similar to that found with the Q_A^- to P^+ electron transfer. In RCs frozen under illumination, the $P^+Q_A^-$ charge recombination rate is almost the same at room and low temperature (12, 13). In RCs frozen in dark, the $P^+Q_A^-$ charge recombination rate is approximately 4-fold slower at room temperature than at low temperature, with much of the change occurring between 180 and 250 K.

The free energy dependence of the Q_A^- to P^+ electron-transfer reaction has been shown to shift as the system is cooled from room temperature to cryogenic temperature (57). Part of this comes from $P^+Q_A^-$ being trapped in a higher energy conformation at low temperature (14). In addition, the reaction reorganization energy is diminished at low temperature because large protein changes become inaccessible (58) at room temperature. The reorganization energy of the Q_B^- to P^+ electron transfer is larger than found for Q_A^- to P^+ (52). The method described here should make it possible to monitor the free energy dependence of the electron transfer from Q_B^- at low temperature to more fully characterize this reaction. A smaller value for the reorganiza-

tion energy would be expected in the light-adapted samples at low temperatures because smaller changes are needed in the light-trapped conformation.

Temperature Dependence of the Electron-Transfer Rate from Q_A^- to Q_B . The electron transfer from Q_A^- to Q_B is measured to be 10^4 s^{-1} at room temperature in native RCs (18, 48, 59–61). The driving force for this reaction can be modified by replacing the native ubiquinone Q_A with other low-potential quinones. The rate is independent of driving force, and so it appears to be limited by a conformational gating step rather than the electron transfer itself (20, 21). The rate of this conformational change decreases with temperature in dark-adapted RCs, indicating that this is an activated process (Figure 11). The loss of quantum yield shows the rate decreases to less than 1 s^{-1} below 200 K. In contrast, the estimated rate of Q_A^- to Q_B electron transfer is faster than 10^3 s^{-1} at 40 K in RCs frozen under illumination so the rate-limiting conformational gate appears to be trapped in the open position in RCs frozen in the light.

In RCs with low-potential Q_{AS} , a faster phase ($>10^5 \text{ s}^{-1}$) was observed for the Q_A^- to Q_B electron transfer. This rate is free energy dependent and so monitors the electron transfer itself, not a conformational change (19). Since the Q_A^- to Q_B electron transfer in RCs frozen in light is likely to be controlled by electron transfer itself, it is more appropriate to compare this rate with the fast phase observed at room temperature. That process has an activation energy of 3.8 kcal/mol (2–25 °C) (18, 19). If temperature is lowered further, this quantum tunneling rate would be predicted to become relatively temperature independent (62, 63). The lack of temperature dependence of the quantum yield in the light-adapted RCs is consistent with a very small activation energy for the reaction.

Electrochromic Shifts Associated with the Q_A^- to Q_B Electron Transfer and with the Trapped Conformational Changes. The electrochromic Stark shifts in the cofactor absorbance bands are caused by changes in the electric field at the cofactor. For Q_A^- to Q_B electron transfer, this is caused by a change in the distance between the negative charge and the cofactors. Part of the shift may also come from the difference in the dielectric screening on the L and M sides of the protein (47).

The electrochromic shifts associated with the Q_A^- to Q_B electron transfer at cryogenic temperature are qualitatively consistent with the kinetically measured difference spectrum at room temperature (18). But because the absorption peaks are narrower at low temperature, the resolution is significantly improved. In addition, the spectrum measured at room temperature will contain contributions from the gating conformational changes and from relaxation after the electron transfer. In contrast, significant conformational changes will already be frozen into the ground state and so will not be seen in the kinetic difference spectrum, and much less relaxation would be expected at cryogenic temperature.

An electrochromic shift associated with the conformational change at low temperature can be observed in the spectrum of the ground state of the RCs frozen in the light and in the dark (Figure 3). The observed shift shows a change in the electric field at the chromophores opposite to the direction of the field produced by the negative charge in $P^+Q_A^-$ or $P^+Q_B^-$ in the active, trapped RC conformation. This more positive field could come from proton uptake, internal proton

movement, or other dielectric responses of residues. These changes would help to stabilize the Q_B^- state and make the electron transfer from Q_A^- to Q_B energetically more favorable. These changes are trapped in the light-adapted RCs and should aid and may be required for the electron transfer from Q_A^- to Q_B .

Relaxation Processes in Frozen RCs. The RCs trapped in the Q_B active conformation can relax slowly to an inactive conformation at temperatures above 120 K. The relaxation in the temperature region 120–200 K results in a slow equilibration between the active and a new inactive state. This relaxed, inactive state is distinct from the dark frozen state as the latter never accesses the active conformation. Thus, only part of the trapped conformational changes can be annealed out in this temperature region. The energy barrier and free energy difference between active and inactive states are quite small. Possible sources of relaxation to this inactive conformation include quinone movement, internal proton shift, or more general dielectric responses of residues nearby. The underlying conformational change makes the formation of $P^+Q_B^-$ energetically unfavorable or very slow (29, 33, 34). Similar relaxation rates of RCs with UQ1 and UQ10 as Q_B suggest that quinone movement is unlikely to be the cause of this relaxation. Quinone translocation between binding sites might be expected to have a higher activation energy and so would freeze out at higher temperature.

Other conformationally unrelaxed states have been previously characterized in RCs. When RCs are frozen under illumination in the absence of Q_B , the protein is also found to be trapped in a light-adapted state, which is indicated by the slower and more distributed $P^+Q_A^-$ charge recombination rate (12, 13). As the RCs are warmed slowly ($>10^3 \text{ s}$), an incomplete relaxation from the light-adapted to the dark-adapted conformation is observed in the 120–200 K temperature region (12, 13). This is the same temperature for relaxation to the partially inactive conformation found here. In addition, the RCs are found to be trapped in an unrelaxed conformation of the product state, $P^+Q_A^-$, below 200 K for the millisecond lifetime of this state (14). The unrelaxed initial product state is at an energy level 200 meV higher (extrapolated to 0 K) than found for the room temperature relaxed state.

Implication for Protein Dynamics. Motions in proteins are often critical for their biological function. The protein energy landscape can be described as a rugged hyperspace with many local minima corresponding to different conformational substates. At room temperature, proteins can fluctuate between substates. But at low temperature, the system is confined to harmonic oscillations near the conformation that it is frozen into.

Here RCs have been shown to be trapped into active or inactive conformational substates depending on the freezing procedure. The partial relaxation of the active state into a previously unobserved inactive conformation shows substates with different enthalpy barriers near the active form. At 120–200 K, the protein is able to overcome only the lower tier of barriers in the light-adapted sample. This transition is to a state separated by only 16 meV from the active light-adapted protein. This would appear to represent a local change in the protein with its own transition temperature. From the elastic incoherent neutron scattering and X-ray crystallography study of bacteriorhodopsin and myoglobin,

the relation between the magnitude of fluctuation and temperature shows that different regions of the protein can have different glass transition temperatures with tiers of barriers having different heights (10, 11). RCs now provide another example for this type of hierarchical organization of energy barriers.

Other conformational changes in RCs caused by freezing under illumination have been previously explored (12, 29, 64–66). The original studies of the Q_A^- to Q_B electron transfer by Kleinfeld et al. suggested a key role for proton binding in the trapped active conformation (12). Measurement of the pH buffering capacity of dark- and light-adapted RCs at room temperature shows that four independent protonatable groups may be involved, with their relative importance changing with pH (65). Theoretical calculations suggest that proton transfer between two acidic residues in the Q_B pocket is required for electron transfer from Q_A^- to Q_B (29). Recent theoretical calculations have highlighted the role of protein dynamics in promoting the electron transfer (66). The measurements presented here show that even very small changes can transform RCs from active to inactive conformations, and factors in addition to quinone movement are important. Changes in RC spectra suggest that active and inactive conformers differ in the intraprotein electrostatic potentials. Future studies determining the temperature dependence of inactivation of both dark- and light-adapted RCs as a function of pH and other parameters may provide a more detailed atomic picture of the energy surface between reactant and product for this reaction.

ACKNOWLEDGMENT

The authors are grateful for stimulating discussions with Drs. Emil Alexov and Armen Mulikidjanian. The His-tagged mutant *Rb. sphaeroides* strain was kindly provided by Drs. Steve Boxer and Alex deWinter. Drs. Maria Luisa Tasayco and Roxana E. Georgescu provided help in purification of the RCs. Mr. Min Xu's aid in the analysis of the kinetic data is also acknowledged.

REFERENCES

- Frauenfelder, H., Sligar, S. G., and Wolynes, P. G. (1991) *Science* 254, 1598–1603.
- Zaccai, G. (2000) *Science* 288, 1604–1607.
- Parak, F., Knapp, E. W., and Kucheida, D. (1982) *J. Mol. Biol.* 161, 177–194.
- Doster, W., Cusack, S., and Petry, W. (1989) *Nature* 337, 754–756.
- Ferrand, M., Dianoux, A. J., Petry, W., and Zaccai, G. (1993) *Proc. Natl. Acad. Sci. U.S.A.* 90, 9668–9672.
- Andreani, C., Filabozzi, A., Menzinger, F., Desideri, A., Deriu, A., and Di Cola, D. (1995) *Biophys. J.* 68, 2519–2523.
- Di Pace, A., Cupane, A., Leone, M., Vitrano, E., and Cordone, L. (1992) *Biophys. J.* 63, 475–484.
- Lonchararich, R. J., and Brooks, B. R. (1990) *J. Mol. Biol.* 215, 439–455.
- Vitcup, D., Ringe, D., Petsko, G. A., and Karplus, M. (2000) *Nat. Struct. Biol.* 7, 34–38.
- Réat, V., Patzelt, H., Ferrand, M., Pfister, C., Oesterhelt, D., and Zaccai, G. (1998) *Proc. Natl. Acad. Sci. U.S.A.* 95, 4970–4975.
- Frauenfelder, H., and McMahon, B. (1998) *Proc. Natl. Acad. Sci. U.S.A.* 95, 4795–4797.
- Kleinfeld, D., Okamura, M. Y., and Feher, G. (1984) *Biochemistry* 23, 5780–5786.
- McMahon, B. H., Muller, J. D., Wraight, C. A., and Nienhaus, G. U. (1998) *Biophys. J.* 74, 2567–2587.
- Xu, Q., and Gunner, M. R. (2000) *J. Phys. Chem. B* 104, 8035–8043.
- Feher, G., Allen, J. P., Okamura, M. Y., and Rees, D. C. (1989) *Nature* 339, 111–116.
- Gunner, M. R. (1991) *Curr. Top. Bioenerg.* 16, 319–367.
- Blankenship, R. E., Madigan, M. T., and Bauer, C. E. (1995) *Anoxygenic Photosynthetic Bacteria*, Vol. 2, Kluwer Academic Publishers, Dordrecht, The Netherlands.
- Tiede, D. M., Vazquez, J., Cordova, J., and Marone, A. P. (1996) *Biochemistry* 35, 10763–10775.
- Li, J., Gilroy, D., Tiede, D. M., and Gunner, M. R. (1998) *Biochemistry* 37, 2818–2829.
- Graige, M. S., Feher, G., and Okamura, M. Y. (1998) *Proc. Natl. Acad. Sci. U.S.A.* 95, 11679–11684.
- Li, J., Takahashi, E., and Gunner, M. R. (2000) *Biochemistry* 39, 7445–7454.
- Utschig, L. M., Ohigashi, Y., Thurnauer, M. C., and Tiede, D. M. (1998) *Biochemistry* 37, 8278–8281.
- Paddock, M. L., Graige, M. S., Feher, G., and Okamura, M. Y. (1999) *Proc. Natl. Acad. Sci. U.S.A.* 96, 6183–6188.
- Schlichting, I., Berendzen, J., Chu, K., Stock, A. M., Maves, S. A., Benson, D. E., Sweet, R. M., Ringe, D., Petsko, G. A., and Sligar, S. G. (2000) *Science* 287, 1615–1622.
- Edman, K., Nollert, P., Royant, A., Belrhali, H., Pebay-Peyroula, E., Hajdu, J., Neutze, R., and Landau, E. M. (1999) *Nature* 401, 822–826.
- Luecke, H., Schobert, B., Richter, H. T., Cartailler, J. P., and Lanyi, J. K. (1999) *Science* 286, 255–261.
- Genick, U. K., Soltis, S. M., Kuhn, P., Canestrelli, I. L., and Getzoff, E. D. (1998) *Nature* 392, 206–209.
- Stowell, M. H. B., McPhillips, T. M., Rees, D. C., Soltis, S. M., Abresch, E., and Feher, G. (1997) *Science* 276, 812–816.
- Alexov, E., and Gunner, M. (1999) *Biochemistry* 38, 8253–8270.
- Grafton, A. K., and Wheeler, R. A. (1999) *J. Phys. Chem.* 103, 5380–5387.
- Alexov, E., Miksovska, J., Baciou, L., Schifer, M., Hanson, D., Sebban, P., and Gunner, M. (2000) *Biochemistry* 39, 5940–5952.
- Beroza, P., Fredkin, D. R., Okamura, M. Y., and Feher, R. (1995) *Biophys. J.* 68, 2233–2250.
- Paddock, M. L., Rongey, S. H., Feher, G., and Okamura, M. Y. (1989) *Proc. Natl. Acad. Sci. U.S.A.* 86, 6602–6606.
- Takahashi, E., and Wraight, C. A. (1992) *Biochemistry* 31, 855–866.
- Goldsmith, J. O., and Boxer, S. G. (1996) *Biochim. Biophys. Acta* 1276, 171–175.
- Clayton, R. K., and Wang, R. T. (1971) *Methods Enzymol.* 23, 696–704.
- Okamura, M. Y., Isaacson, R. A., and Feher, G. (1975) *Proc. Natl. Acad. Sci. U.S.A.* 72, 3492–3496.
- Woodbury, N. W., Parson, W. W., Gunner, M. R., Prince, R. C., and Dutton, P. L. (1986) *Biochim. Biophys. Acta* 851, 6–22.
- McComb, J. C., Stein, R. R., and Wraight, C. A. (1990) *Biochim. Biophys. Acta* 1015, 156–171.
- Gunner, M. R., Robertson, D. E., and Dutton, P. L. (1986) *J. Phys. Chem.* 90, 3783–3795.
- Steinbach, P. J., Chu, K., Frauenfelder, H., Johnson, J. B., Lamb, D. C., Nienhaus, G. U., Sauke, T. B., and Young, R. D. (1992) *Biophys. J.* 61, 235–245.
- Tikhonov, A. N., and Arsenin, V. Y. (1977) *Solutions of ill-posed problems*, Wiley, New York.
- Gunner, M. R., and Dutton, P. L. (1989) *J. Am. Chem. Soc.* 111, 3400–3412.
- Mancino, L. J., Dean, D. P., and Blankenship, R. E. (1984) *Biochim. Biophys. Acta* 764, 46–54.
- McElroy, J. D., Mauzerall, D. C., and Feher, G. (1974) *Biochim. Biophys. Acta* 333, 261–277.
- Breton, J. (1988) in *The photosynthetic bacterial reaction center: structure and dynamics* (Breton, J., and Vermegio, A., Eds.) pp 59–69, Plenum, New York and London.

47. Steffen, M. A., Lao, K., and Boxer, S. G. (1994) *Science* 264, 810–816.
48. Kleinfeld, D., Okamura, M. Y., and Feher, G. (1984) *Biochim. Biophys. Acta* 766, 126–140.
49. Labahn, A., Paddock, M. L., McPherson, P. H., Okamura, M. Y., and Feher, G. (1994) *J. Phys. Chem.* 98, 3417–3423.
50. Takahashi, E., and Wraight, C. A. (1992) *Biochemistry* 31, 855–866.
51. Labahn, A., Bruce, J. M., Okamura, M. Y., and Feher, G. (1995) *Chem. Phys.* 97, 355–366.
52. Allen, J. P., Williams, J. C., Graige, M., Paddock, M. L., Labahn, A., Feher, G., and Okamura, M. Y. (1998) *Photosynth. Res.* 55, 227–233.
53. Paddock, M. L., Rongey, S. H., McPherson, P. H., Juth, A., Feher, G., and Okamura, M. Y. (1994) *Biochemistry* 33, 734–745.
54. Shopes, R. J., and Wraight, C. A. (1987) *Biochim. Biophys. Acta* 893, 409–425.
55. Franzen, S., and Boxer, S. G. (1993) *J. Phys. Chem.* 97, 6304–6318.
56. Sebban, P. (1988) *Biochim. Biophys. Acta* 936, 124–132.
57. Ortega, J. M., Mathis, P., Williams, J. C., and Allen, J. P. (1996) *Biochemistry* 35, 3354–3361.
58. Dutton, P. L., and Moser, C. C. (1994) *Proc. Natl. Acad. Sci.* 91, 10247–10250.
59. Vermeglio, A., and Clayton, R. K. (1977) *Biochim. Biophys. Acta* 461, 159–165.
60. Wraight, C. A. (1979) *Biochim. Biophys. Acta* 548, 309–327.
61. Takahashi, E., Maroti, P., and Wraight, C. A. (1992) in *Electron and Proton Transfer in Chemistry and Biology* (Muller, A., Ed.) pp 219–236, Elsevier, New York.
62. Marcus, R. A., and Sutin, N. (1985) *Biochim. Biophys. Acta* 811, 265–322.
63. DeVault, D. (1980) *Q. Rev. Biophys.* 13, 387–564.
64. Brzezinski, P., and Andreasson, L. E. (1995) *Biochemistry* 34, 7498–7506.
65. Kalman, L., Sebban, P., Hanson, D. K., Schiffer, M., and Maroti, P. (1998) *Biochim. Biophys. Acta* 1365, 513–521.
66. Balabin, I. A., and Onuchic, J. N. (2000) *Science* 290, 114–117.

BI002326Q